

MILLIMETER IMAGING OF THE β PICTORIS DEBRIS DISK: EVIDENCE FOR A PLANETESIMAL BELT

DAVID J. WILNER¹, SEAN M. ANDREWS¹, AND A. MEREDITH HUGHES^{2,3}

¹ Harvard-Smithsonian Center for Astrophysics, 60 Garden Street, Cambridge, MA 02138, USA

² Department of Astronomy, 601 Campbell Hall, University of California, Berkeley, CA 94720, USA

Received 2010 November 19; accepted 2010 December 9; published 2011 January 12

ABSTRACT

We present observations at 1.3 mm wavelength of the β Pictoris debris disk with beam size $4''.3 \times 2''.6$ (83×50 AU) from the Submillimeter Array. The emission shows two peaks separated by $\sim 7''$ along the disk plane, which we interpret as a highly inclined dust ring or belt. A simple model constrains the belt center to 94 ± 8 AU, close to the prominent break in slope of the optical scattered light. We identify this region as the location of the main reservoir of dust-producing planetesimals in the disk.

Key words: circumstellar matter – planetary systems – planet–disk interactions – stars: individual (β Pictoris)

Online-only material: color figures

1. INTRODUCTION

The discovery of excess far-infrared emission from the nearby (19.44 ± 0.05 pc; van Leeuwen 2007) A6V-type main-sequence star β Pictoris (Aumann 1985) together with optical imaging of scattered light from circumstellar dust (Smith & Terrile 1984) established the “debris disk” paradigm where dust grains orbiting the star originate from an eroding reservoir of larger bodies (see reviews by, e.g., Artymowicz 1997; Backman & Paresce 1993; Wyatt 2008). The nearly edge-on disk surrounding this young star (12^{+8}_{-4} Myr; Zuckerman et al. 2001) is relatively luminous ($F_{\text{disk}}/F_{\star} = 2.5 \times 10^{-3}$; Lagrange et al. 2000) and has been studied in great detail with a panoply of observational techniques. High-resolution images in the optical (Kalas & Jewitt 1995; Heap et al. 2000; Golimowski et al. 2006), near-infrared (Mouillet et al. 1997a; Tamura et al. 2006; Boccaletti et al. 2009), and mid-infrared (Wahhaj et al. 2003; Weinberger et al. 2003; Okamoto et al. 2004; Telesco et al. 2005) all show a wealth of structure, including density concentrations, an inner cavity, and asymmetries such as warps. These features, including a secondary disk of scattered light inclined by about 5° (Ahmic et al. 2009), have been variously ascribed to the gravitational influence of a giant planet or planets (e.g., Mouillet et al. 1997b; Augereau et al. 2001; Freistetter et al. 2007; Kennedy & Wyatt 2010). Indeed, a planetary mass companion at a projected distance of 8 AU from the star now has been directly imaged (Lagrange et al. 2009, 2010).

The emerging view of debris disks like β Pictoris postulates the presence of a planetesimal belt that produces dust with a range of sizes through collisional cascades (Strubbe & Chiang 2006; Wyatt 2008; Kuchner & Stark 2010). The stirring of the planetesimals may be due to the gravity of ~ 1000 km sized objects formed within the belt (Kenyon & Bromley 2004), or due to the presence of planets located closer to the star (Moro-Martín et al. 2008). In either case, the dynamical effects of stellar radiation create a distribution of grain sizes that depends on distance from the star, e.g., the blow-out of the smallest “ β -meteoroid” grains. An important consequence is that images of debris disks at different wavelengths are dominated by different grain sizes and can appear remarkably different (Wyatt 2006). Observations at millimeter wavelengths are most sensitive to large grains that are minimally affected by radiative forces

and thus have the potential to trace best the location of the dust-producing parent planetesimals. The debris disk around Vega, for example, shows a clumpy ring confined to radii < 200 AU at wavelengths of $350 \mu\text{m}$ and longward (Holland et al. 1998; Wilner et al. 2002; Marsh et al. 2006), while it appears smooth and featureless and extends to radii ~ 800 AU in mid-infrared light that arises predominantly from small grains expelled by radiation (Su et al. 2005). The debris disk around HR 8799, an A-type star that harbors three directly imaged planets, shows similar morphological changes with wavelength (Su et al. 2009).

For the β Pictoris debris disk, the angular resolutions of (sub-)millimeter images have been too coarse to reveal much structure. Images from several different telescopes generally show dust emission extended along a position angle of $\sim 30^{\circ}$, consistent with the optical disk: JCMT/SCUBA at $850 \mu\text{m}$ with a $14''$ beam (Holland et al. 1998), APEX/LABOCA at $870 \mu\text{m}$ with an $18''$ beam (Nilsson et al. 2009), SEST/SIMBA at $1200 \mu\text{m}$ with a $24''$ beam (Liseau et al. 2003), and Herschel/SPIRE at 250, 350, and $500 \mu\text{m}$ with $18''$, $25''$, and $37''$ beams, respectively (Vandenbussche et al. 2010). A separate peak or blob of dust emission is also found $\sim 30''$ to the southwest of the star, but the relationship of this peak to the main disk is unclear; Dent et al. (2000) and Vandenbussche et al. (2010) have suggested that it is a background galaxy with a coincidental alignment with the disk plane.

Millimeter interferometry offers a way to obtain higher angular resolution and more information on the largest detectable grain populations within the debris disk. In this Letter, we present imaging observations of β Pictoris at 1.3 mm wavelength from the Submillimeter Array (SMA)⁴ that reveal a belt of emission around the star centered near a radius of ~ 95 AU that likely marks a reservoir of planetesimals.

2. OBSERVATIONS

We used the eight-element SMA (Ho et al. 2004) on Mauna Kea, Hawaii, to observe β Pictoris in the compact-north configuration (baselines 6–97 m) on 2010 August 9 and in the extended configuration (baselines 12–178 m) on 2010 September 1. The phase center was chosen to be $\alpha =$

³ Miller Fellow.

⁴ The Submillimeter Array is a joint project between the Smithsonian Astrophysical Observatory and the Academia Sinica Institute of Astronomy and Astrophysics and is funded by the Smithsonian Institution and the Academia Sinica.

$5^{\text{h}}47^{\text{m}}17^{\text{s}}.09$, $\delta = -51^{\circ}03'59''.5$ (J2000), about $0''.9$ from the stellar position at the epoch of the observations. The β Pictoris system is a challenging target for the SMA as it never rises above 20° elevation. Nonetheless, usable data were obtained in both configurations over the hour angle range ± 1.7 . The weather conditions were good on both days, with 225 GHz atmospheric opacities 0.07–0.09 and stable atmospheric phase. The correlator was configured to provide the maximum 4 GHz of bandwidth in each of two sidebands centered ± 6 GHz from a central local oscillator frequency of 235.6 GHz (wavelength of 1.3 mm), with a uniform spectral resolution of 0.8125 MHz. At this frequency, the primary beam size is $\sim 54''$ (FWHM). Observations of the strong source 3C454.3 obtained at the start of each track were used to calibrate the passband response. Observations of the quasars J0538-440 and J0522-364 were interleaved with β Pictoris in order to calibrate time-dependent gain variations. The astrometric uncertainty is $\lesssim 0''.3$. The absolute flux scale was set with reference to observations of the standard calibrator Callisto in each track and should be accurate to better than 15%. The calibration procedure was performed using the IDL based MIR software. Subsequent imaging and deconvolution were done within the MIRIAD package.

3. RESULTS AND ANALYSIS

3.1. 1.3 mm Emission

Figure 1 shows a contour image of the 1.3 mm emission overlaying a *Hubble Space Telescope*/Space Telescope Imaging Spectrograph (STIS) coronagraphic image of optical scattered light from Heap et al. (2000). The 1.3 mm image was made using natural weighting and a modest taper in the east–west direction to avoid extreme ellipticity of the synthesized beam, which is $4''.3 \times 2''.6$ (83×50 AU) oriented nearly north–south (position angle 2°). The maximum sidelobes of the dirty beam obtained with this weighting scheme are located about $13''$ to the east and west, with amplitude 15% of the central peak. The rms noise in this image is 0.6 mJy beam $^{-1}$. The star symbol is plotted offset by $(0''.35, 0''.70)$ from the phase center, within the uncertainties of the stellar position corrected for proper motion. The 1.3 mm emission shows two peaks at positions symmetrically offset from the stellar position by $\sim 3''.5$ to the northeast and southwest, respectively. This basic morphology suggests a highly inclined ring or belt, where the peaks are due to limb brightening at the ansae (where the column density is highest). While the southwest peak appears slightly brighter, the difference lies within the noise and cannot be considered significant.

Because the SMA observations are not sensitive enough to detect the stellar photosphere, the alignment of the images from the SMA and *Hubble Space Telescope* is limited by the absolute astrometry. Even taking account of this uncertainty, it seems that the two millimeter emission peaks do not align perfectly along the 30° position angle of the primary optical disk (Kalas & Jewitt 1995). Instead, examination of Figure 1 suggests that the peaks align more closely with the 34° position angle of the scattered light secondary disk described by Golimowski et al. (2006). Observations with better resolution and sensitivity are needed to confirm this suggestion; the noncircular beam makes it difficult to assess small differences in orientation, and the millimeter emission structure itself may prove to be warped or more complex.

The 1.3 mm flux in the detected structure is 13 ± 1.4 mJy, estimated by integrating over the emission in the image. This

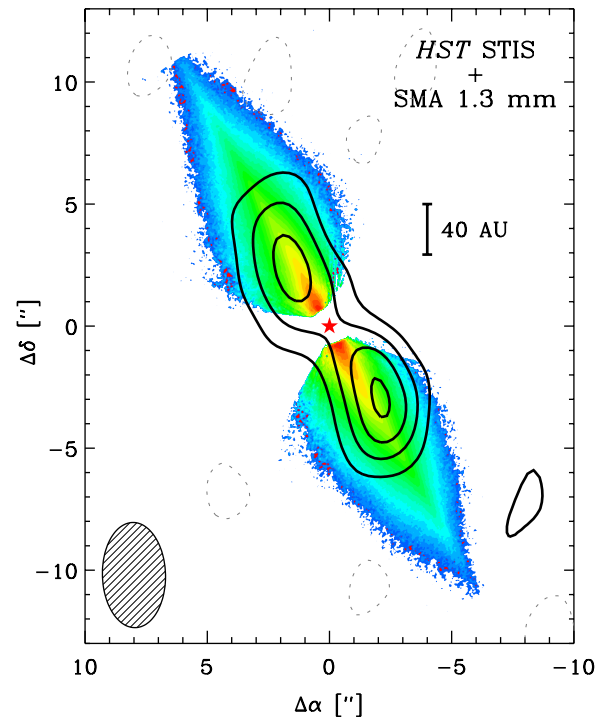


Figure 1. SMA image of the 1.3 mm continuum emission from β Pictoris overlaid on an image of optical scattered light from Heap et al. (2000). The contour levels are $-2, 2, 4, 6, \dots \times 0.6$ mJy (the rms noise level). Negative contours are dotted. The ellipse in the lower left corner represents the $4''.3 \times 2''.6$ (FWHM) synthesized beam size. The star symbol indicates the location of the stellar photosphere.

(A color version of this figure is available in the online journal.)

value is only approximately half of the 24.3 ± 3.0 mJy measured in the $24''$ SEST beam at 1.2 mm (Liseau et al. 2003), a discrepancy significantly larger than expected from the mutual absolute calibration uncertainties and the spectral slope. The difference suggests the presence of an additional, extended 1.3 mm emission component, missed in these observations by the spatial filtering properties of the interferometer. Given the shortest SMA baselines, the peak brightness is diminished already by 50% for a $20''$ (FWHM) Gaussian source (Wilner & Welch 1994), a size scale smaller than the SEST beam. Judging from the partially resolved images from far-infrared and submillimeter filled aperture telescopes, this missing component is likely elongated along the disk, which extends beyond the SMA field of view.

The separate dust peak to the southwest is detected at $\sim 5\sigma$, offset by $(-21''.4 \pm 0''.4, -22''.4 \pm 0''.6)$ from the center of the field (not shown). The corresponding absolute position is $\alpha = 5^{\text{h}}47^{\text{m}}14^{\text{s}}.82$, $\delta = -51^{\circ}04'21''.9$ (J2000). Because the primary beam correction is large and uncertain at this location beyond the half-power point, it is difficult to provide an accurate estimate of the flux. The position is well determined, however, and shows that this peak does not lie along an extension of the optical disk. This supports previous suggestions that this feature is a background source, presumably a dusty galaxy.

3.2. Belt Location and Width

We constrain the basic properties of the 1.3 mm emission with a simple model that assumes the structure is characterized by a flat, axisymmetric belt of emission. We take the radial profile of the emission to be $r^{-0.5}$, which is physically motivated by optically thin emission for constant surface density and a

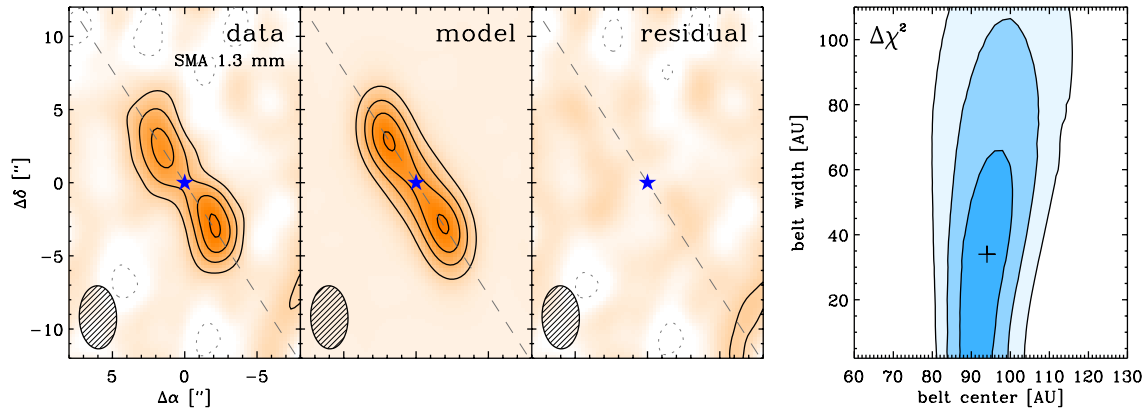


Figure 2. Left panels: SMA image of the 1.3 mm emission from β Pictoris together with the image of the best-fit axisymmetric belt model and the residuals. The contour levels and beam size are the same as in Figure 1. The dashed line indicates a position angle of 34° . Right panel: the χ^2 surface for the belt center and width model parameters, with contours at 1σ , 2σ , 3σ . The cross marks the best-fit model.

(A color version of this figure is available in the online journal.)

temperature profile of $r^{-0.5}$ due to stellar irradiation. We fix the inclination and orientation of the belt on the sky to 87° and 33° , respectively; due to the limited resolution, small variations in these geometric parameters do not have significant effects on the results. This simple model has three parameters: the belt center R , belt width ΔR , and flux F . We calculate a grid of models over the parameter ranges $60 \text{ AU} < R < 130 \text{ AU}$ and $2 \text{ AU} < \Delta R < 110 \text{ AU}$ in steps of 2 AU and $10 \text{ mJy} < F < 17 \text{ mJy}$ in steps of 0.5 mJy, and calculate χ^2 values for each model using all of the SMA visibilities. The right panel of Figure 2 shows the resulting χ^2 surface (marginalized over the parameter F). The cross marks the best fit at $R = 94 \pm 8 \text{ AU}$, $\Delta R = 34^{+44}_{-32} \text{ AU}$, and $F = 15 \pm 2 \text{ mJy}$; the uncertainties represent the formal 1σ errors. The data strongly constrain the belt center location and allow for widths up to sizes comparable to the resolution of the observations. The three left panels of Figure 2 show the 1.3 mm image from Figure 1 together with images of the best-fit model and the residuals, all made in the same way. The model reproduces the main features of the data, and the residuals are consistent with noise. If a steeper radial emissivity were assumed, then the outer edge of the emission could extend further. However, a belt with a width that encroaches much closer to the star than the best fit may be difficult to reconcile with the mid-infrared emission from the system. A proper model that considers the constraints of the full spectral energy distribution requires many more assumptions than made here, in particular about the grain composition, grain size distribution, collisional behaviors, and dynamics.

4. DISCUSSION

The new millimeter observations improve substantially on previous single-dish images and start to resolve fine structure in the β Pictoris disk. Since large grains cannot travel far from their place of origin due to short grain-grain collisional timescales and negligible radiation effects, the emission at this long wavelength should trace the dust-producing planetesimals. Inspection and analysis of the resolved millimeter emission suggest a highly inclined ring or belt centered at a radius within or near $\sim 95 \text{ AU}$. Aside from the nearly edge-on viewing geometry, the millimeter morphology is strikingly similar to other well-studied A-type stars with substantial circumstellar dust, in particular Vega (e.g., Marsh et al. 2006) and Fomalhaut (e.g., Holland et al. 2003). The region interior to this belt in β Pictoris is clearly not empty, as evidenced by mid-infrared

imaging and spectroscopy (e.g., Telesco et al. 2005; Chen et al. 2007), but it must be relatively deficient in dust mass or millimeter-sized grains or both.

The location of the millimeter emission belt corresponds closely to a prominent break in the slope of the optical scattered light, as well as a change in the optical color gradient (Golimowski et al. 2006). These properties are plausibly explained in a model with dust-producing planetesimals located just interior the break, with stellar radiation (and possibly also a stellar wind) creating a radial gradient in grain size (Augereau et al. 2001; Strubbe & Chiang 2006). In this scenario, the extended halo of emission along the disk plane would be dominated by a population of small grains blown out onto highly elliptical or hyperbolic orbits, possibly with temperatures above the local blackbody values, that cover a large area on the sky and give rise to the fraction of millimeter emission missed by the interferometer.

One implication of the multi-component emission structure is that the far-infrared to millimeter spectral index of 2.34 ± 0.07 indicated by the integrated spectrum (Vandenbussche et al. 2010) may not be representative of any of the individual components. Depending on the details, it is possible, for example, that the belt component could show a steeper spectral index that would be closer to expectations for a steady-state collisional cascade, without resorting to unusual fragmentation prescriptions or wavy grain size distributions (Thébault & Augereau 2007). Until multi-wavelength observations are available in this regime that clearly resolve the relevant structures, it will be problematic to use the integrated spectral index to make conclusive inferences about the grain properties and size distributions.

The 1.3 mm image of the dust belt around β Pictoris sets the stage for much improved future observations with the Atacama Large Millimeter/Submillimeter Array (ALMA), now under construction in Chile (and much better placed for aperture synthesis observations of this southern source). More detailed millimeter images have the potential to determine, e.g., if the dust belt center is offset from the star, or if the emission exhibits pericenter glow or other asymmetries that could point to dynamical perturbations from additional planets in this remarkable system.

We thank the SMA staff for scheduling and executing the two filler tracks that provided the data used in this Letter. We

also thank Sally Heap and Don Linder for providing the *Hubble Space Telescope*/STIS coronagraphic image in FITS format. A.M.H. is supported by a fellowship from the Miller Institute for Basic Research in Science.

Facility: SMA

REFERENCES

- Ahmic, M., Croll, B., & Artymowicz, P. 2009, *ApJ*, **705**, 529
 Artymowicz, P. 1997, *Annu. Rev. Earth Planet. Sci.*, **25**, 175
 Augereau, J. C., Nelson, R. P., Lagrange, A. M., Papaloizou, J. C. B., & Mouillet, D. 2001, *A&A*, **370**, 447
 Aumann, H. H. 1985, *PASP*, **97**, 885
 Backman, D. E., & Paresce, F. 1993, in *Protostars and Planets III*, ed. E. H. Levy & J. I. Lunine (Tucson, AZ: Univ. Arizona Press), 1253
 Boccaletti, A., Augereau, J., Baudoz, P., Pantin, E., & Lagrange, A. 2009, *A&A*, **495**, 523
 Chen, C. H., et al. 2007, *ApJ*, **666**, 466
 Dent, W. R. F., Walker, H. J., Holland, W. S., & Greaves, J. S. 2000, *MNRAS*, **314**, 702
 Freistetter, F., Krivov, A. V., & Löhne, T. 2007, *A&A*, **466**, 389
 Golimowski, D. A., et al. 2006, *AJ*, **131**, 3109
 Heap, S. R., Lindler, D. J., Lanz, T. M., Cornett, R. H., Hubeny, I., Maran, S. P., & Woodgate, B. 2000, *ApJ*, **539**, 435
 Ho, P. T. P., Moran, J. M., & Lo, K. Y. 2004, *ApJ*, **616**, L1
 Holland, W. S., et al. 1998, *Nature*, **392**, 788
 Holland, W. S., et al. 2003, *ApJ*, **582**, 1141
 Kalas, P., & Jewitt, D. 1995, *AJ*, **110**, 794
 Kennedy, G. M., & Wyatt, M. C. 2010, *MNRAS*, **405**, 1253
 Kenyon, S. J., & Bromley, B. C. 2004, *AJ*, **127**, 513
 Kuchner, M. J., & Stark, C. C. 2010, *AJ*, **140**, 1007
 Lagrange, A., Backman, D. E., & Artymowicz, P. 2000, in *Protostars and Planets IV*, ed. V. Mannings, A. P. Boss, & S. S. Russell (Tucson, AZ: Univ. Arizona Press), 639
 Lagrange, A., et al. 2009, *A&A*, **493**, L21
 Lagrange, A., et al. 2010, *Science*, **329**, 57
 Liseau, R., Brandeker, A., Fridlund, M., Olofsson, G., Takeuchi, T., & Artymowicz, P. 2003, *A&A*, **402**, 183
 Marsh, K. A., Dowell, C. D., Velusamy, T., Grogan, K., & Beichman, C. A. 2006, *ApJ*, **646**, L77
 Moro-Martin, A., Wyatt, M. C., Malhotra, R., & Trilling, D. E. 2008, in *Kuiper Belt*, ed. A. Barucci et al. (Tucson, AZ: Univ. Arizona Press), 465
 Mouillet, D., Lagrange, A., Beuzit, J., & Renaud, N. 1997a, *A&A*, **324**, 1083
 Mouillet, D., Larwood, J. D., Papaloizou, J. C. B., & Lagrange, A. M. 1997b, *MNRAS*, **292**, 896
 Nilsson, R., Liseau, R., Brandeker, A., Olofsson, G., Risacher, C., Fridlund, M., & Pilbratt, G. 2009, *A&A*, **508**, 1057
 Okamoto, Y. K., et al. 2004, *Nature*, **431**, 660
 Smith, B. A., & Terrile, R. J. 1984, *Science*, **226**, 1421
 Strubbe, L. E., & Chiang, E. I. 2006, *ApJ*, **648**, 652
 Su, K. Y. L., et al. 2005, *ApJ*, **628**, 487
 Su, K. Y. L., et al. 2009, *ApJ*, **705**, 314
 Tamura, M., Fukagawa, M., Kimura, H., Yamamoto, T., Suto, H., & Abe, L. 2006, *ApJ*, **641**, 1172
 Telesco, C. M., et al. 2005, *Nature*, **433**, 133
 Thébault, P., & Augereau, J. 2007, *A&A*, **472**, 169
 Vandenbussche, B., et al. 2010, *A&A*, **518**, L133
 van Leeuwen, F. 2007, *A&A*, **474**, 653
 Wahhaj, Z., Koerner, D. W., Ressler, M. E., Werner, M. W., Backman, D. E., & Sargent, A. I. 2003, *ApJ*, **584**, L27
 Weinberger, A. J., Becklin, E. E., & Zuckerman, B. 2003, *ApJ*, **584**, L33
 Wilner, D. J., Holman, M. J., Kuchner, M. J., & Ho, P. T. P. 2002, *ApJ*, **569**, L115
 Wilner, D. J., & Welch, W. J. 1994, *ApJ*, **427**, 898
 Wyatt, M. C. 2006, *ApJ*, **639**, 1153
 Wyatt, M. C. 2008, *ARA&A*, **46**, 339
 Zuckerman, B., Song, I., Bessell, M. S., & Webb, R. A. 2001, *ApJ*, **562**, L87